Grain boundary wetting in the NdFeB-based hard magnetic alloys

B. B. Straumal, Yu. O. Kucheev, I. L. Yatskovskaya, I. V. Mogilnikova, G. Schütz, A. N. Nekrasov & B. Baretzky

Journal of Materials Science
Full Set - Includes `Journal of Materials Science Letters'

ISSN 0022-2461
Volume 47
Number 24

J Mater Sci (2012) 47:8352-8359
DOI 10.1007/s10853-012-6618-5

Springer

J Mater Sci (2012) 47:8352–8359
DOI 10.1007/s10853-012-6618-5

HTC 2012

Grain boundary wetting in the NdFeB-based hard magnetic alloys

B. B. Straumal · Yu. O. Kucheev · I. L. Yatskovskaya · I. V. Mogilnikova · G. Schütz · A. N. Nekrasov · B. Baretzky

Received: 28 April 2012 / Accepted: 25 May 2012 / Published online: 13 June 2012

Abstract Since the end of 1980s, NdFeB-based hard magnetic alloys have been the materials with the highest available magnetic performance. NdFeB-based magnets are produced either by liquid-phase sintering or by melt spinning. In the present investigation, NdFeB alloys quenched after annealing in the semi-liquid state are used to study the wetting of $Nd_2Fe_{14}B$ grain boundaries by a Nd-rich liquid phase. It is shown that a transition from partial wetting to complete wetting occurs with increasing temperature. The results are compared with the data in the literature for NdFeB-based alloys processed by liquid-phase sintering. The relation between wetting properties and magnetic performance of these alloys is also discussed.

B. B. Straumal (✉) · Yu. O. Kucheev · I. L. Yatskovskaya · I. V. Mogilnikova
Institute of Solid State Physics, Russian Academy of Sciences, Chernogolovka, Russia 142432
e-mail: straumal@issp.ac.ru; straumal@mf.mpg.de

B. B. Straumal · Yu. O. Kucheev · I. V. Mogilnikova
National University of Science and Technology "MISiS", Leninsky Prospect 4, Moscow, Russia 119991

B. B. Straumal · G. Schütz
Max-Planck Institut für Intelligente Systeme (Former Institut für Metallforschung), Heisenbergstraße 3, 70569 Stuttgart, Germany

B. B. Straumal · B. Baretzky
Karlsruher Institut für Technologie (KIT), Institut für Nanotechnologie, Hermann-von-Helmholtz-Platz 1, 76344 Eggenstein-Leopoldshafen, Germany

A. N. Nekrasov
Institute of Experimental Mineralogy, Russian Academy of Sciences, Chernogolovka, Moscow, Russia 142432

Introduction

For a liquid droplet on a solid substrate, two situations are possible. If the liquid spreads on the surface, then this is a case of full (or complete) wetting. The contact angle θ between the liquid and the solid is zero. If the liquid droplet forms a finite contact angle, then wetting is partial (or incomplete). Cahn [1] and Ebner and Saam [2] first showed that the (reversible) transition from partial to complete wetting can take place with increasing temperature and that this transition is a true surface-phase transformation. Reviews on wetting-phase transitions can be found in [3–7]. Cahn's theory was originally developed for multi-component systems presenting a critical transformation (miscibility gap). However, by analogy, Cahn's theory can also be applied to the phenomenon of grain boundary wetting.

The transition from partial to complete wetting can be observed within grain boundaries (GBs) if the GB energy σ_{GB} becomes higher than $2\sigma_{SL}$ where σ_{SL} is the solid–liquid energy (Fig. 1). The first results, showing that GBs can be wetted perfectly by a liquid alloy, were obtained for the Zn–Sn, Zn–Sn–Pb and Ag–Pb systems using polycrystalline solids [8, 9]. Later, the original experimental data were reconsidered applying, by analogy, Cahn's point-of-view to the GB wetting phenomenon [10]. Subsequently, numerous results, obtained also using polycrystalline solids, have indicated the occurrence of GB wetting-phase transformations, particularly for the Zn–Sn, Al–Cd, Al–In, Al–Pb [11 and references therein] and W–Ni, W–Cu, W–Fe, Mo–Ni, Mo–Cu, Mo–Fe systems [12 and references therein]. Accurate measurements of the temperature dependence of the GB/liquid alloy contact angle and of the temperature of complete wetting (noted T_w) have been made using individual GBs in specially grown bicrystals for the Cu–In [13], Al–Sn [14],

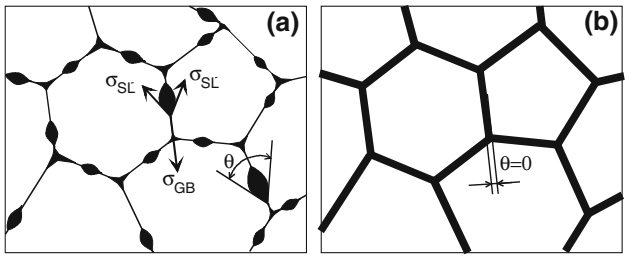

Fig. 1 Diagram of a polycrystalline solid with grain boundaries **a** partially wetted and **b** completely wetted by a liquid phase (*black*). When the grain boundary energy σ_{GB} becomes higher than $2\sigma_{SL}$ (σ_{SL} being the solid–liquid interfacial energy), the contact angle θ becomes zero

Zn–Sn [15], Al–Zn [16], Sn–Bi [17], In–Sn [18], Zn–Sn and Zn–In [19] systems. The second-phase wetting the GBs can also be a crystalline solid, as in the Zn–Al [20], Al–Zn [21], Al–Mg [22] and Co–Cu [23] alloys, or even an amorphous phase [24–27]. All these surfaces and GB wetting-phase transformations are of the first order (discontinuous), which means that the first temperature derivative of surface (or GB) energy is discontinuous at T_w. However, wetting transitions of a higher order are also possible. In this case, the first temperature derivative of surface (or GB) energy varies continuously around T_w, but second temperature derivative presents a break. Continuous wetting-phase transitions were theoretically predicted in [28–30] and for a long time had remained a topic of very intensive theoretical investigations [31–34] (see also the review [7]). Experimentally, a continuous wetting-phase transition was first observed for liquids only in 1996 [35, 36]. Later, continuous wetting-phase transitions were observed for liquid/liquid systems of technological importance for oil recovery, consisting of alkanes in contact with methanol, water or brine [37–41]. For GBs, a continuous wetting-phase transition was observed for the first time in the Zn–Al system [16].

Cahn's generic phase diagram also predicted that the tie-line of the wetting transition in the two-phase region continues in the single-phase (solid solution) area as a prewetting line [1]. Between the prewetting line and the solidus line, the surface contains a thin (only a few nm) liquid-like layer of a phase which is not stable as a bulk phase. Experimental evidence for such prewetting (or premelting) layers was also found for GBs in metallic systems Fe–Si–Zn [42–45], Cu–Bi [46–48], Al–Zn [49] and W–Ni [50, 51] and in ceramics Al_2O_3 [52–56], Y_2O_3-doped AlN [57], La-doped $SrTiO_3$ [58], Bi_2O_3-doped ZnO [59, 60] and Ca-doped Si_3N_4 [61]. Prewetting was also observed for interphase boundaries [62–68]. Wetting- and prewetting (premelting)-phase transformations drastically change GB properties such as diffusivity [43–46], mobility [69], ductility [46, 70], segregation [46–48] and electrical conductivity [71].

GB wetting phenomena play an important role in liquid-phase sintering of metals and ceramics [72, 73], in processing of metal matrix composites by semi-solid routes [74], in thixotropic casting [75], in liquid metal heat-exchangers used in nuclear technology [76], etc. An important alloy processed mainly by liquid-phase sintering is the Nd–Fe–B alloy. Nd–Fe–B-sintered magnets have been developed over the last 25 years for advanced applications due to their excellent magnetic properties [77]. In Nd–Fe–B-sintered magnets, the ferromagnetic $Nd_2Fe_{14}B$ matrix phase is basically surrounded by a Nd-rich intergranular phase [78]. The degree of separation of ferromagnetic $Nd_2Fe_{14}B$ grains by the paramagnetic layer of the

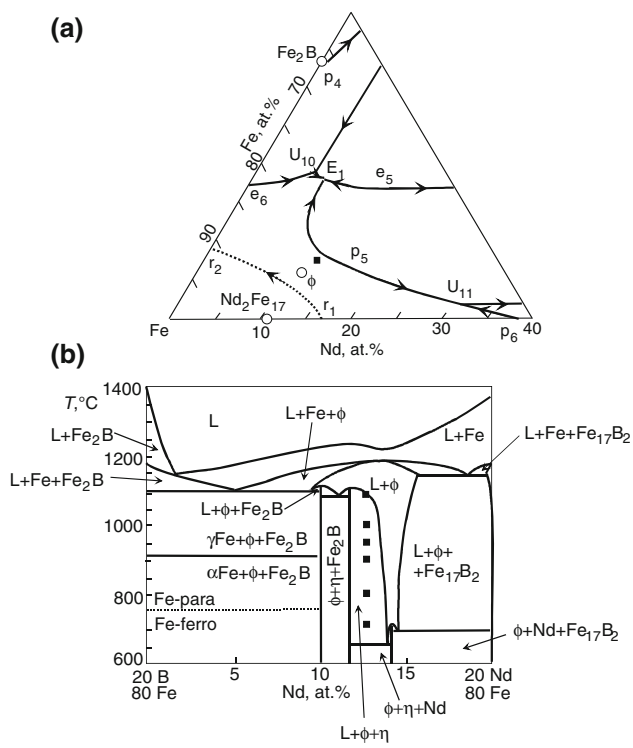

Fig. 2 **a** Liquidus projection close to the Fe-corner of the Fe–Nd–B phase diagram [79]. *Open circles* mark the Fe_2B, Nd_2Fe_{17} and $Fe_{14}Nd_2B$ (ϕ) binary and ternary compounds. The composition of the investigated alloy is shown by the *solid square*. E_1 is the ternary eutectic point $L = \gamma Fe + Fe_{14}Nd_2B + Fe_7Nd_2B_6$ at 1,090 °C. e_5 is the eutectic point $L = Fe_{14}Nd_2B + Fe_7Nd_2B_6$ (η) at 1,095 °C. e_6 is the eutectic point $L = \gamma Fe + Fe_2B$ at 1,177 °C. U_{10} is the transformation $L + Fe_2B = \gamma Fe + Fe_7Nd_2B_6$ (η). U_{11} is the transformation $L + \gamma Fe = Nd_2Fe_{17} + Fe_{14}Nd_2B$. p_4 is the peritectic point $L + FeB = Fe_2B$ at 1,407 °C. p_5 is the peritectic point $L + \gamma Fe = Fe_{14}Nd_2B$ at 1,407 °C. p_6 is the peritectic point $L + \gamma Fe = Fe_{17}Nd_2$ at 1,185 °C. r_1 is the remelting point $\delta Fe = L + \gamma Fe$ at 1,392 °C. r_3 is the remelting point $\delta Fe = L + \gamma Fe$ at 1,381 °C. **b** The 80 at.% Fe section of the Fe–Nd–B phase diagram [80, 81]. The composition of the investigated alloy and annealing temperatures are shown by *solid squares*

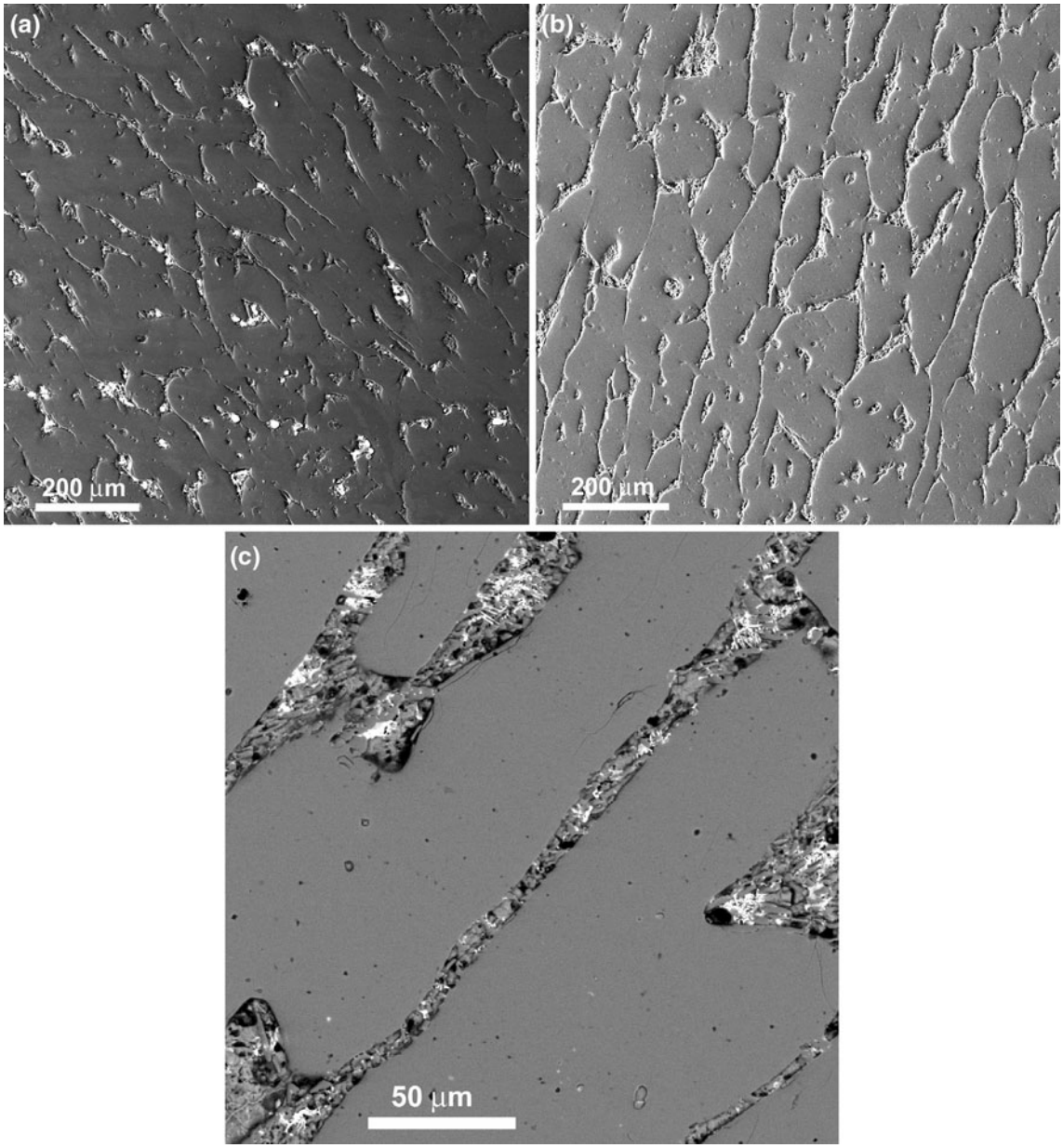

Fig. 3 SEM micrographs of a Fe–12.3at.%Nd–7.6at.%B alloy annealed at **a** 900 °C, **b** 1,000 °C and **c** 1,100 °C, 2 h. The $Fe_{14}Nd_2B$ (ϕ phase) grains (matrix) appear *dark-grey*. The Nd-rich hcp phase between $Fe_{14}Nd_2B$ grains appears *light-grey*. Pores (artefact of sample preparation) appear *black*. Fine particles of $Nd_2Fe_7B_6$ (η-phase) between $Fe_{14}Nd_2B$ grains appear *white*

Nd-rich phase is critically important for their superior magnetic performance. The NdFeB-based permanent magnets are able to store large amounts of magnetic energy. Their product $(B_dH_d)_{max}$ is up to 512 kJ/m^3, where B_d is the remnant induction (the magnetic induction that remains in a magnetic material after removal of an applied saturating magnetic field), and H_d is the demagnetizing force. Therefore, it is very important to investigate accurately the wetting of $Nd_2Fe_{14}B$ GBs by the Nd-rich liquid phase. This was the aim of the present study.

Experimental

The Fe–12.3at.%Nd–7.6at.%B alloy was investigated. This composition is close to that of the most important magnetic compound $Fe_{14}Nd_2B$ in the Fe–Nd–B system (Fig. 2) [79–81]. The alloy was prepared from high-purity components (5 N Fe, 4 N Nd and 4 N B) by vacuum induction melting. Two-mm-thick slices were cut from ϕ 10-mm cylindrical Fe–Nd–B ingots and sealed inside evacuated silica ampoules with a residual pressure of approximately

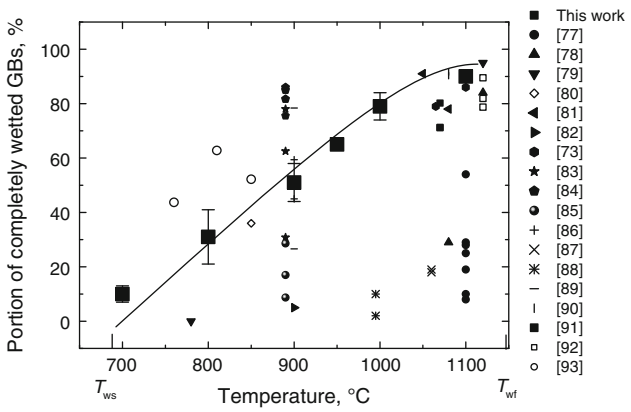

Fig. 4 Temperature dependence for the fraction of $Fe_{14}Nd_2B$ GBs completely wetted by the Nd-rich phase (*large full squares*, *thick line*). $T_{ws} = 690 \pm 10$ °C and $T_{wf} = 1{,}150 \pm 10$ °C are, respectively, the temperatures of the beginning and end of the GB wetting-phase transition of $Fe_{14}Nd_2B$ GBs by the Nd-rich liquid phase. The *large filled squares* represent the results obtained in this study. The *small symbols* are the results obtained by analysing the data from the literature for liquid-state sintering samples. For each *symbol*, the reference to the original study is also given

4×10^{-4} Pa at room temperature. Samples were annealed at temperatures of 700, 800, 900, 950, 1000 and 1100 °C for 2 h and then quenched in water. The accuracy of the annealing temperature was ±2 °C. After quenching, samples were embedded in 'Technovit' resin and then mechanically ground and polished, using 1 μm diamond paste in the last polishing step, for metallographic study. After etching, samples were examined by light microscopy and scanning electron microscopy (SEM). SEM investigations were carried out in a Tescan Vega TS5130 MM microscope equipped using the INCA Energy 350 energy dispersive spectrometer produced by Oxford Instruments. Light microscopy was performed using a Neophot-32 light microscope equipped with 10-Mpix Canon Digital Rebel XT camera. A quantitative analysis of the wetting transition was performed by adopting the following criterion: a $Fe_{14}Nd_2B$ GB was considered to be completely wetted only when a film of Nd-rich liquid had filled the whole GB (Figs. 1b, 3c); if this film appeared to be interrupted, then the GB was considered to be partially wetted (Figs. 1a, 3a, b). At least 300 GBs were analysed at each temperature. Typical micrographs obtained by SEM are shown in Fig. 3.

Results and discussion

SEM micrographs of the Fe–12.3at.%Nd–7.6at.%B alloy annealed at 900, 1000 and 1100 °C are shown in Fig. 3. The $Fe_{14}Nd_2B$ (ϕ-phase) grains (matrix) appear dark-grey. The Nd-rich hcp phase between $Fe_{14}Nd_2B$ grains appears light-grey. Pores (artefact of sample preparation) appear black. Fine particles of $Nd_2Fe_7B_6$ (η-phase) between $Fe_{14}Nd_2B$ grains appear white. In Fig. 3a, b both completely and partially wetted $Fe_{14}Nd_2B$ GBs are visible. The elongated areas of the Nd-rich phase form chains along the partially wetted $Fe_{14}Nd_2B$ GBs (Fig. 3a, b). A majority of $Fe_{14}Nd_2B$ GBs are completely wetted by the Nd-rich phase. In this case, the Nd-rich phase forms a continuous network separating the $Fe_{14}Nd_2B$ grains. At annealing temperatures of 700, 800, 900, 950, 1000 and 1100 °C, the Fe–12.3at.%Nd–7.6at.%B alloy studied consists of three phases (see phase diagram in Fig. 2) [79–81]. The major part of the alloy volume is occupied by $Fe_{14}Nd_2B$ (ϕ phase) grains. The remaining volume is an intergranular Nd-rich liquid phase containing particles of the $Nd_2Fe_7B_6$ (η) solid phase clearly visible in Fig. 3c where these particles appear as finely dispersed white precipitates.

Figure 4 shows the temperature dependence for the fraction of $Fe_{14}Nd_2B$ GBs completely wetted by the Nd-rich phase (large full squares, thick line). At 700 °C, only about 10 % of $Fe_{14}Nd_2B$ GBs are completely wetted. By extrapolating the solid line towards 0 %, the starting temperature of the GB wetting-phase transition is estimated to be $T_{ws} = 690 \pm 10$ °C. At 1,100 °C, about 90 % of $Fe_{14}Nd_2B$ GBs are completely wetted. By extrapolating the solid line towards 100 %, the finishing temperature T_{wf} of the GB wetting-phase transition is estimated to be $T_{wf} = 1{,}150 \pm 10$ °C. Therefore, above this temperature, all the $Fe_{14}Nd_2B$ GBs are perfectly wetted by the Nd-rich liquid alloy.

At each temperature above $T_{ws} = 690 \pm 10$ °C, both completely and partially wetted GBs exist. Most probably this difference is due to the variations in specific enthalpy (excess energy per unit area) of different $Fe_{14}Nd_2B$ GBs. For example, it was noted earlier that low-energy GBs (such as twin GBs) cannot be completely wetted by a second solid phase and contain only chains of solid particles instead of a continuous second phase layer [19]. The increase in the amount of completely wetted GBs with increasing temperature can be explained by the fact that GBs with different energies also have different temperatures of wetting transition T_w. For example, GBs with higher energy have a lower T_w [12, 13].

In addition to our results (large filled squares), Fig. 4 shows the data from the literature obtained by analysing published micrographs of NdFeB-based alloys. Only micrographs containing at least 100 grains were used for this analysis. The main differences between our samples and those in the literature are the processing method and the purity of the alloys. Our samples were processed by quenching semi-liquid alloys obtained from high-purity Nd, Fe and B. The final microstructure consists of large grains (up to ~500 μm). The data from the literature are for samples processed by liquid-phase sintering of powders

Table 1 Composition and heat treatment of alloys processed by liquid-phase sintering selected from the literature for calculating the amount of wetted grain boundaries

Composition (subscripts in at.%)	Liquid-phase sintering temperature T_{ls} and duration	First post-sintering annealing temperature T_1 and duration	Second post-sintering annealing temperature T_2 and duration	References
$Pr_{14}Fe_{80}B_6$, $Pr_{14}Fe_{79.9}B_6Nb_{0.1}$, $Pr_{14}Fe_{75.9}Co_4B_6Nb_{0.1}$, $Pr_{14}Fe_{71.9}Co_8B_6Nb_{0.3}$, $Pr_{14}Fe_{69.9}Co_{10}B_6Nb_{0.1}$, $Pr_{14}Fe_{67.9}Co_{12}B_6Nb_{0.3}$, $Pr_{14}Fe_{63.9}Co_{16}B_6Nb_{0.3}$	1,100 °C, 2 h	600 °C, 1 h		[82]
$Nd_{12.8}Fe_{79.8}B_{7.4}$	1,080 °C, 1 h 1,120 °C, 1 h	600 °C, 1 h		[83]
$Nd_{15.5}Dy_{1.0}Fe_{72.7}Co_{3.0}B_{6.8}Al_{1.0}$	780 °C (SHS)	1,000 °C, 1 h		[84]
$Nd_{15.5}Dy_{1.0}Fe_{72.7}Co_{3.0}B_{6.8}Al_{1.0}$	1,120 °C, 1 h	600 °C, 1 h		[84]
$Nd_{14}Fe_{60}Co_{18}B_7Ga_{1.0}$	780 °C, 0.5 h	850 °C, 0.5 h		[85]
$(NdDy)_{14}(FeCoAl)_{80}B_6$	1,050 °C 1,080 °C			[86]
$Nd_{14.54}Fe_{74.2}Co_{4.9}B_{6.36}$	1,090 °C, 1 h	900 °C, 1 h	500–650 °C, 1 h	[87]
$Fe_{81.11}(NdDy)_{12.99}B_{5.9}$	1,065 °C, 3 h	900 °C, 2 h	600 °C, 3 h	[78]
$Fe_{80.85}(NdDy)_{12.99}B_{5.75}Al_{0.24}Ga_{0.1}Zr_{0.07}$	1,105 °C, 3 h	900 °C, 2 h	600 °C, 3 h	[78]
$(Pr, Nd)_{14.8}Fe_{78.7}B_{6.5} + Al_{100-x}Cu_x$ ($x = 15, 35, 45$)	1,100 °C, 2 h	890 °C, 3 h	480 °C, 2 h	[88]
$Fe_{68.43}Nd_{28.2}Dy_{2.0}Al_{0.1}Nb_{0.2}Ga_{0.11}B_{0.96}$ + 0, 0.2, 0.3 or 0.5 wt% ($Cu_{60}Zn_{40}$)	1,090 °C, 2 h	890 °C, 2 h	500 °C, 3 h	[89]
$Fe_{78.7}(Pr, Nd)_{14.8}B_{6.5}$ $Fe_{78.7}(Pr, Nd)_{14.8}B_{6.5}$ + 0.6 wt% $Al_{85}Cu_{15}$	1,090 °C, 2 h	890 °C, 2 h	550 °C, 3 h	[90]
$Fe_{80.20}Nd_{13.79}(AlGaNbZr)_{0.48}B_{5.53}$ $Fe_{79.57}Nd_{13.79}(AlGaNbZr)_{0.48}B_{6.16}$	1,090 °C, 2 h	900 °C, 2 h	560 °C, 3 h	[91]
$Fe_{76}Pr_{16}B_8$	1,060 °C, 1 h			[92]
$Fe_{76}Pr_{16}B_8$	1,060 °C, 1 h	1,000 °C, 24 h		[92]
$Fe_{78.2}Nd_{12.5}Pr_{2.3}B_{6.3}Al_{0.6}Cu_{0.1}$	995 °C, 1 h	800 °C, 1 h	600 °C, 1 h + 540 °C, 1 h	[93]
$Fe_{78.2}Nd_{12.5}Pr_{2.3}B_{6.3}Al_{0.6}Cu_{0.1}$	945 °C, 1 h	800 °C, 1 h	600 °C, 1 h + 540 °C, 1 h	[93]
$(Fe_{68.64}Nd_{29.3}Dy_{0.5}Tb_{0.2}Al_{0.1}Ga_{0.11}Nb_{0.1}Zr_{0.1}B_{0.95})_{100-x}$ Cu ($x = 0, 0.05, 0.1$ and 0.2)	1,105 °C, 2 h	900 °C, 2 h	510 °C, 3 h	[94]
$Fe_{77}Nd_{15}Dy_{1.2}Al_{0.8}B_6$ + 0 or 0.1 at.% MgO	1,080 °C, 2 h	900 °C, 2 h	560 °C, 2 h	[95]
$Fe_{71}Nd_{22}B_7$ + 0.4 at.% MgO or ZnO	1,040–1,100 °C, 2 h	900 °C, 2 h	600 °C, 2 h	[96]
$Fe_{66.35}Nd_{29.5}Dy_{2.0}B_{1.1}Al_{0.25}Gd_{0.8}$ + 0, 0.1, 0.2 or 0.4 at.% MgO	1,120 °C, 2.5 h	510 °C, 3 h		[97]
$Fe_{78}Nd_{15}Dy_{1.2}Al_{0.8}B_6$	760, 810 or 850 °C, 40 MPa, 10 min	1,000 °C, 2 h		[98]

at a temperature T_{ls}. The samples contain additives (see Table 1) and have small grains (a few micrometres). After sintering, the samples were annealed for 0.5–3 h at one and in some cases two temperatures lower than T_{ls} (Table 1). The results are given in Fig. 4 along with small symbols together with the reference to the original study. Figure 4 clearly shows that in most cases, the percentage of completely wetted $Fe_{14}Nd_2B$ GBs is lower than in our samples.

In order to obtain NdFeB-based alloys with good hard magnetic properties, it is critically important for the $Fe_{14}Nd_2B$ grains to be perfectly separated from each other by a non-ferromagnetic layer. Figure 3c clearly displays that in some locations, the $Nd_2Fe_7B_6$ (η) particles form 'bridges' connecting the $Fe_{14}Nd_2B$ grains across the liquid intergranular Nd-rich layer. According to the data from the literature, the η-phase is ferromagnetic [99]. Ferromagnetic bridges of η-phase can detrimentally influence the magnetic properties. These ferromagnetic bridges in the paramagnetic intergranular layers have to be excluded in the industrial hard magnetic FeNdB-alloys. On the other hand, to obtain the magnetic separation by a non-magnetic layer, the thickness of this layer must be greater than the width of a Bloch wall between magnetic domains (about 5 nm) [100]. It would appear that the magnetic separation of the

$Fe_{14}Nd_2B$ grains can be obtained not only by macroscopically thick (a few μm to 100 nm) layers of a wetting phase but also by thin layers of a prewetting/premelting phase [42–68]. The presence of such nanometre-thick layers in the NdFeB-based alloys has been documented on several occasions [101–107]. The exact thermodynamic conditions of their formation are still unclear and need to be studied in the future.

It has been found empirically that the additional short annealing of liquid-phase sintered alloys slightly below the eutectic temperature $T_{e2} = 665$ °C [79] increases the coercivity of the material [78, 83–99]. It is generally believed that this is because the additional annealing improves the magnetic separation of the $Fe_{14}Nd_2B$ grains. However, below T_{e2} no liquid phase is present in the FeNdB-based alloys. This means that the phase(s) wetting the $Fe_{14}Nd_2B$ GBs should be solid.

Liquid-phase sintering is not the only method that can be used to produce NdFeB-based permanent magnets. In other technologies, the NdFeB-based alloys are quickly quenched from the liquid phase by melt spinning [105–107]. The amorphous or amorphous + nanocrystalline ribbons obtained are pressed together with a binder and heat treated to obtain the optimum structure and magnetic properties. Moreover, as a result of severe plastic deformation, the mixture of amorphous and nanocrystalline phases can also be obtained in the NdFeB-based alloys [107, 108]. It seems that even after a relatively long annealing time, the remaining amorphous phase separates the $Fe_{14}Nd_2B$ grains. In this case, the amorphous phase probably also 'wets' the $Fe_{14}Nd_2B$ GBs like, for example, in nanograined ferromagnetic ZnO films [23, 24, 27].

Conclusions

1. The Nd-rich liquid phase can wet the $Fe_{14}Nd_2B$ GBs either completely or partially.
2. The percentage of completely wetted $Fe_{14}Nd_2B$ GBs increases from 10 % (at 700 °C) to almost 100 % (at 1,100 °C). The estimated start and end temperatures of the GB wetting-phase transition are $T_{ws} = 690 \pm 10$ °C and $T_{wf} = 1{,}150 \pm 10$ °C, respectively.
3. The Nd-rich liquid phase between $Fe_{14}Nd_2B$ grains and at three GB junctions contains finely dispersed particles of the ferromagnetic η-phase ($Nd_2Fe_7B_6$). These particles can build ferromagnetic bridges between $Fe_{14}Nd_2B$ grains within intergranular Nd-rich layers and, therefore, detrimentally influence the magnetic properties. These ferromagnetic bridges must be excluded from industrial hard magnetic FeNdB-alloys.

Acknowledgements The authors thank the Allianz Industrie Forschung (project FE.5150.0028.4067), Max-Planck Institut für Intelligente Systeme (Stuttgart), the Programme of Creation and Development of the National University of Science and Technology 'MISiS', the Russian Foundation for Basic Research (grants 10-02-00086, 11-03-00029 and 11-08-90439) and the Ukrainian Fundamental Research State Fund (grant Φ28.2107) for their financial support.

References

1. Cahn JW (1977) J Chem Phys 66:3667
2. Ebner C, Saam WF (1977) Phys Rev Lett 38:1486
3. de Gennes PG (1985) Rev Mod Phys 57:827
4. Sullivan DE, Telo da Gama MM (1986) In: Croxton CA (ed) Fluid interfacial phenomena. Wiley, New York
5. Dietrich S (1988) In: Domb C, Lebowitz JL (eds) Phase transitions and critical phenomena, vol 12. Academic Press, London
6. Schick M (1990) In: Charvolin J, Joanny J-F, Zinn-Justin J (eds) Liquids at interfaces (Les Houches Session XLVIII, 1988). Elsevier, Amsterdam
7. Bonn D, Ross D (2001) Rep Prog Phys 64:1085
8. Passerone A, Eustathopoulos N, Desré P (1977) J Less-Common Met 52:37
9. Passerone A, Sangiorgi R, Eustathopoulos N (1982) Scripta Metall 16:547
10. Rabkin EI, Shvindlerman LS, Straumal BB (1991) Int J Mod Phys B 5:2989
11. Eustathopoulos N (1983) Int Met Rev 28:189
12. Straumal BB (2003) Grain boundary phase transitions. Nauka Publishers, Moscow (in Russian)
13. Straumal B, Muschik T, Gust W, Predel B (1992) Acta Metall Mater 40:939
14. Straumal B, Molodov D, Gust W (1995) Interface Sci 3:127
15. Straumal B, Gust W, Watanabe T (1999) Mater Sci Forum 294–296:411
16. Straumal BB, Gornakova AS, Kogtenkova OA, Protasova SG, Sursaeva VG, Baretzky B (2008) Phys Rev B 78:054202
17. Yeh C-H, Chang L-S, Straumal BB (2011) J Mater Sci 46:1557. doi:10.1007/s10853-010-4961-y
18. Yeh C-H, Chang L-S, Straumal BB (2010) Mater Trans 51:1677
19. Gornakova AS, Straumal BB, Tsurekawa S, Chang L-S, Nekrasov AN (2009) Rev Adv Mater Sci 21:18
20. López GA, Mittemeijer EJ, Straumal BB (2004) Acta Mater 52:4537
21. Protasova SG, Kogtenkova OA, Straumal BB, Zięba P, Baretzky B (2011) J Mater Sci 46:4349. doi:10.1007/s10853-011-5322-1
22. Straumal BB, Baretzky B, Kogtenkova OA, Straumal AB, Sidorenko AS (2010) J Mater Sci 45:2057. doi:10.1007/s10853-009-4014-6
23. Straumal BB, Kogtenkova OA, Straumal AB, Kuchyeyev YuO, Baretzky B (2010) J Mater Sci 45:4271. doi:10.1007/s10853-010-4377-8
24. Straumal BB, Protasova SG, Mazilkin AA, Myatiev AA, Straumal PB, Schütz G, Goering E, Baretzky B (2010) J Appl Phys 108:073923
25. Straumal BB, Myatiev AA, Straumal PB, Mazilkin AA, Protasova SG, Goering E, Baretzky B (2010) JETP Lett 92:396
26. Mazilkin AA, Abrosimova GE, Protasova SG, Straumal BB, Schütz G, Dobatkin SV, Bakai AS (2011) J Mater Sci 46:4336. doi:10.1007/s10853-011-5304-3
27. Straumal BB, Mazilkin AA, Protasova SG, Myatiev AA, Straumal PB, Goering E, Baretzky B (2011) Thin Solid Films 519:1192

28. Dietrich S, Schick M (1985) Phys Rev B 31:4718
29. Saam WF, Shenoy VB (1995) J Low Temp Phys 101:225
30. Shenoy VB, Saam WF (1995) Phys Rev Lett 75:4086
31. Dietrich S, Napiorkowski M (1991) Phys Rev A 43:1861
32. Indekeu JO, van Leeuwen JMJ (1995) Physica C 251:290
33. Indekeu JO, van Leeuwen JMJ (1997) Physica A 236:114
34. Boulter CJ, Clarysse F (1999) Phys Rev E 60:R2472
35. Ragil K, Meunier J, Broseta D, Indekeu JO, Bonn D (1996) Phys Rev Lett 77:1532
36. Shahidzadeh N, Bonn D, Ragil K, Broseta D, Meunier J (1998) Phys Rev Lett 80:3992
37. Ross D, Bonn D, Meunier J (1999) Nature 400:737
38. Pfohl T, Riegler H (1999) Phys Rev Lett 82:783
39. Bertrand E, Dobbs H, Broseta D, Indekeu JO, Bonn D, Meunier J (2000) Phys Rev Lett 85:1282
40. Rafaï S, Bonn D, Bertrand E, Meunier J, Weiss VC, Indekeu JO (2004) Phys Rev Lett 92:245701
41. Rafaï S, Bonn D, Meunier J (2005) Physica A 358:97
42. Semenov VN, Straumal BB, Glebovsky VG, Gust W (1995) J Cryst Growth 151:180
43. Rabkin EI, Semenov VN, Shvindlerman LS, Straumal BB (1991) Acta Metall Mater 39:627
44. Noskovich OI, Rabkin EI, Semenov VN, Straumal BB, Shvindlerman LS (1991) Acta Metall Mater 39:3091
45. Straumal BB, Noskovich OI, Semenov VN, Shvindlerman LS, Gust W, Predel B (1992) Acta Metall Mater 40:795
46. Chang L-S, Rabkin E, Straumal BB, Baretzky B, Gust W (1999) Acta Mater 47:4041
47. Chang L-S, Rabkin E, Straumal BB, Hoffmann S, Baretzky B, Gust W (1998) Def Diff Forum 156:135
48. Schölhammer J, Baretzky B, Gust W, Mittemeijer E, Straumal B (2001) Interface Sci 9:43
49. Straumal BB, Mazilkin AA, Kogtenkova OA, Protasova SG, Baretzky B (2007) Phil Mag Lett 87:423
50. Gupta VK, Yoon DH, Meyer HM, Luo J (2007) Acta Mater 55:3131
51. Luo J, Gupta VK, Yoon DH, Meyer HM (2005) Appl Phys Lett 87:231902
52. Luo J, Dillon SJ, Harmer MP (2009) Microsc Today 17:22
53. Cho J, Wang CM, Chan HM, Rickman JM, Harmer MP (2002) J Mater Sci 37:59. doi:10.1023/A:1013185506017
54. Dillon SJ, Tang M, Carter WC, Harmer MP (2007) Acta Mater 55:6208
55. Dillon SJ, Harmer MP (2007) Acta Mater 55:5247
56. Dillon SJ, Harmer MP (2008) J Eur Ceram Soc 28:1485
57. Pezzotti G, Nakahira A, Tajika M (2000) J Eur Ceram Soc 20:1319
58. Furukawa Y, Sakurai O, Shinozaki K, Mizutani N (1996) J Ceram Soc Jpn 104:900
59. Elfwing M, Osterlund R, Olsson E (2000) J Am Ceram Soc 83:2311
60. Wang H, Chiang Y-M (1998) J Am Ceram Soc 81:89
61. Tanaka I, Kleebe HJ, Cinibuluk MK, Bruley J, Clarke DR, Ruhle M (1998) J Am Ceram Soc 77:911
62. Baram M, Kaplan WD (2006) J Mater Sci 41:7775. doi:10.1007/s10853-006-0897-7
63. Baram M, Chatain D, Kaplan WD (2011) Science 332:206
64. Scheu C, Dehm G, Kaplan WD (2001) J Am Ceram Soc 84:623
65. Avishai A, Kaplan WD (2005) Acta Mater 53:1571
66. Avishai A, Scheu C, Kaplan WD (2005) Acta Mater 53:1559
67. Avishai A, Kaplan WD (2004) Zt Metallkde 95:266
68. Baram M, Garofalini SH, Kaplan WD (2011) Acta Mater 59:5710
69. Molodov DA, Czubayko U, Gottstein G, Shvindlerman LS, Straumal BB, Gust W (1995) Phil Mag Lett 72:361
70. Valiev RZ, Murashkin MY, Kilmametov A, Straumal BB, Chinh NQ, Langdon TG (2010) J Mater Sci 45:4718. doi:10.1007/s10853-010-4588-z
71. Straumal BB, Sluchanko NE, Gust W (2001) Defect Diffusion Forum 188–190:185
72. Islam SH, Qu X, He X (2007) Powder Metall 50:11
73. Wei DQ, Meng QC, Jia DC (2007) Ceram Int 33:221
74. Solek KP, Kuziak RM, Karbowniczek M (2007) Arch Metall Mater 52:25
75. Ji ZS, Hu ML, Zheng XP (2007) J Mater Sci Technol 23:247
76. Shatilla YA, Loewen EP (2005) Nucl Technol 151:239
77. Sagawa M, Fujimura S, Togawa N, Yamamoto H, Matsuura Y (1984) J Appl Phys 55:2083
78. Yu LQ, Zhong XL, Zhang YP, Yan YG, Zhen YH, Zakotnik M (2011) J Magn Magn Mater 323:1152
79. Matsuura Y, Hirosawa Y, Yamamoto H, Fujimura S, Sagawa M, Osamura K (1985) Jpn J Appl Phys 24:L635
80. Schneider G, Henig E-T, Petzow G, Stadelmaier HH (1986) Zt Metallkunde 77:755
81. Knoch KG, Reinsch B, Petzow G (1994) Zt Metallkunde 85:5
82. Barbosa LP, Takiishi H, Faria RN (2004) J Magn Magn Mater 268:232
83. Madaah Hosseini HR, Kianvash A (2004) J Magn Magn Mater 281:92
84. Yue M, Zhang JX, Liu WO, Wang GP (2004) J Magn Magn Mater 271:364
85. Yue M, Liu X, Xiao Y, Zhang JX (2004) J Magn Magn Mater 269:227
86. Pei W, He C, Lian F, Zhou G, Yang H (2002) J Magn Magn Mater 239:475
87. Gabay AM, Zhang Y, Hadjipanais GC (2002) J Magn Magn Mater 238:226
88. Yan M, Ni J, Ma T, Ahmad Z, Zhang P (2011) Mater Chem Phys 126:195
89. Wu Y, Ni J, Ma T, Yan M (2010) Physica B 405:3303
90. Ni JJ, Ma TY, Cui XG, Wu YR, Yan M (2010) J Alloys Compd 502:346
91. Yu LQ, Zhang YP, Fu QT (2009) Adv Mater Res 79–82:1043
92. Corfield MR, Harris IR, Williams AJ (2010) J Magn Magn Mater 322:36
93. Li WF, Ohkubo T, Hono K, Sagawa M (2009) J Magn Magn Mater 321:1100
94. Cui XG, Yan M, Ma TY, Yu LQ (2008) Physica B 403:4182
95. Mo W, Zhang L, Shan A, Cao L, Wu J, Komuro M (2008) J Alloys Compd 461:351
96. Mo W, Zhang L, Liu Q, Shan A, Wu J, Komuro M, Shen L (2008) J Rare Earths 26:268
97. Yu LQ, Zhang J, Hu SQ, Han ZD, Yan M (2008) J Magn Magn Mater 320:1427
98. Mo W, Zhang L, Shan A, Cao L, Wu J, Komuro M (2007) Intermetallics 15:1483
99. Fidler J (1985) IEEE Trans Magn 21:1955
100. Kronmüller H (2007) Handbook of magnetism and advanced magnetic materials. Wiley, Chichester
101. Komuro M, Satsu Y, Suzuki H (2010) Mater Sci Forum 638–642:1357
102. Ma Y, Liu Y, Li J, Li C, Chu L (2010) J Magn Magn Mater 322:2419
103. Zern A, Seeger M, Bauer J, Kronmüller H (1998) J Magn Magn Mater 184:89

104. Li S, Gu B, Bi H, Tian Z, Xie G, Zhu Y, Du Y (2002) J Appl Phys 19:7514
105. Liu ZW, Huang HY, Gao XX, Yu HY, Zhong XC, Zhu J, Zeng DC (2011) J Phys D 44:025003
106. Thielsch J, Hinz D, Schultz L, Gutfleisch O (2010) J Magn Magn Mater 322:3208
107. Stolyarov VV, Gunderov DV, Popov AG, Puzanova TZ, Raab GI, Yavari AR, Valiev RZ (2002) J Magn Magn Mater 242–245:1399
108. Stolyarov VV, Gunderov DV, Valiev RZ, Popov AG, Gaviko VS, Ermolenko AS (1999) J Magn Magn Mater 196–197:166